







# A Two-Stage Multi-Layer Perceptron for High-Resolution DOA Estimation

Yanjun Zhang , Yan Huang , *Member, IEEE*, Jun Tao , *Senior Member, IEEE*, Shiyang Tang , *Member, IEEE*, Hing Cheung So , *Fellow, IEEE*, and Wei Hong , *Fellow, IEEE*

**Abstract**—Nowadays, with the development of automotive and traffic radars, a higher angle resolution is required for an increasing demand of four-dimensional (4D) imaging radar. In this paper, the high-precision direction-of-arrival (DOA) estimation problem is solved by using a deep learning (DL) framework. Most existing on-grid DL-based methods have an upper limit of one-degree resolution. The DOA estimation performance under such resolution is still far behind conventional methods, and is not accurate enough in practical applications. Hence, we introduce a two-stage multi-layer perceptron (TS-MLP) framework to achieve higher resolution of DOA estimation with low complexity by dividing the problem into two main parts. The first MLP is used to determine the coarse grid point nearest to the source angle, and the second MLP fine tunes the estimate within the coarse grids. In addition, we propose a solution to the source association problem between the two stages when handling multiple targets. Our scheme shows much higher accuracy compared with existing DL-based methods, and has comparable performance with traditional high-resolution methods. Moreover, it performs quite robust in the presence of array imperfections.

**Index Terms**—Direction-of-arrival (DOA) estimation, deep learning (DL), two-stage multi-layer perceptron (TS-MLP), super resolution.

## I. INTRODUCTION

**D**IRECTION-OF-ARRIVAL (DOA) estimation has been an important research problem with a long history in array antenna systems, including radar and wireless communications [1]. The main applications of automotive radar include target detection, tracking, and imaging. After transmitting signals through the array antenna, the received target echo

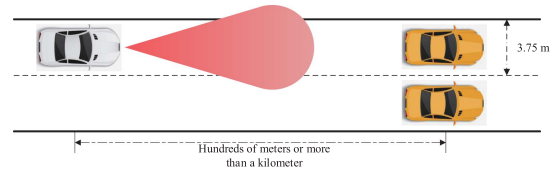


Fig. 1. Automotive radars target detection.

signals are processed to obtain the range, speed, angle, and other information of targets. The DOA estimation of signal is an important part of it. It is usually carried out for the target echo signal of the same range-velocity bin. The number of such targets is usually not large, but there is a high requirement for the real-time and resolution of DOA estimation. In automotive radar systems, the DOA resolution is limited by the aperture of an antenna array, then improving the accuracy is always one of the dominant directions. In this paper, we mainly focus on the requirements of fast high-resolution DOA estimation. For example, the existing automotive radar can realize DOA estimation with a physical-aperture resolution of about  $0.5^\circ$  at a high cost, which is not enough to distinguish traffic lanes or even vehicles at a long distance, as shown in Fig. 1, so a higher resolution of less than  $0.1^\circ$  is necessary without increasing the physical aperture.

Early DOA estimation approach is digital beamforming (DBF), whose angular resolution is limited by the physical array aperture, i.e., the Rayleigh limit [2]. Up to now, subspace-based methods have been a standard approach for DOA estimation. These methods can breakthrough the Rayleigh limit and realize super-resolution estimation. The classic one is the multiple signal classification (MUSIC) algorithm, proposed in 1986 [3]. However, the high computational complexity brought by the eigenvalue decomposition process makes it difficult to apply to the radar system with low computational power. On this basis, root-MUSIC (RMUSIC) was proposed in [4] to estimate DOAs by figuring out the root of the equivalent polynomial of the spectrum. Another successful subspace-based method is the estimation of signal parameters via rotational invariance (ESPRIT) algorithm [5], [6], which realizes super-resolution performance through the rotation invariance between subarrays. Although the ESPRIT method avoids peak search compared to MUSIC, it requires sub-arrays with the same structure. Other commonly used DOA estimation methods include maximum likelihood (ML) [7], min-norm [8], weighted subspace fitting (WSF) [9]. The above methods are still widely studied and

Manuscript received 16 February 2023; revised 27 July 2023; accepted 11 February 2024. Date of publication 22 February 2024; date of current version 16 July 2024. This work was supported in part by the National Natural Science Foundation of China under Grant 62271142, Grant 62271138, and Grant U20B2039, in part by the Shanghai Academy of Space Technology Innovation under Grant SAST2021-043, and in part by the Zhishan Young Scholar Funding of Southeast University. The review of this article was coordinated by Prof. Joongheon Kim. (*Corresponding author: Yan Huang.*)

Yanjun Zhang, Yan Huang, and Wei Hong are with the State Key Laboratory of Millimeter Waves, School of Information Science and Engineering, Southeast University, Nanjing 211100, China, and also with the Purple Mountain Laboratory, Nanjing 211100, China (e-mail: yellowstone0636@hotmail.com).

Jun Tao is with the Key Laboratory of Underwater Acoustic Signal Processing of the Ministry of Education, School of Information Science and Engineering, Southeast University, Nanjing 210096, China.

Shiyang Tang is with the National Laboratory of Radar Signal Processing, Xidian University, Xi'an 710071, China.

Hing Cheung So is with the Department of Electrical Engineering, City University of Hong Kong, Hong Kong.

The demo code is available in <https://github.com/Whisperzyj/TS-MLP>.

Digital Object Identifier 10.1109/TVT.2024.3368451

improved nowadays [10], [11], but they also have the problem of high computational complexity [12], [13].

Deep learning (DL), which originates from the M-P model [14], is now dominating the artificial intelligence domain, no matter computer vision (CV) or natural language processing (NLP) [15]. The concept of perceptron was firstly proposed in [16], then corresponding training algorithm and nonlinear mapping were developed for multi-layer perceptron (MLP) [17]. With the rapid development of computer technology in recent years, DL has become a very attractive research direction.

DOA estimation is also a key technology in massive multiple-input multiple-output (MIMO) communication systems. It is not only important for the recovery of channel state information (CSI) and beamforming, but also assists the security of physical layer. In this field, DL has been applied successfully. The deep neural network (DNN) in [18] can estimate the DOAs of massive MIMO signals with the received signal vector and incorporate the estimated DOA into the complex gain information to realize channel estimation. A novel radial-basis function neural network (RBFNN), which has obvious advantages over subspace-based method, was proposed in [19], achieving accurate estimation under high-speed motion and tracking nonlinear changes of DOAs. In addition, since it is difficult to obtain numerous training samples in practice, transfer learning was explored in DOA estimation for wireless communications in [20]. The above works aim to better transmit information in wireless communication systems, while in automotive radars, the purpose of DOA estimation is to achieve more accurate target sensing. Several DOA estimation methods based on the DL framework have been proposed [21], [22], [23], [24], [25], [26], [27], [28], [29], [30], [31], [32], [33], [34], and improved performance is demonstrated for various situations including coherent signals [25], [33], [34], low signal-to-noise ratio (SNR) [21], [26], and array imperfections [24], [25]. Compared with traditional methods, DL for DOA estimation has several unique advantages. First, the DL-based method is data-driven so that it is unconstrained by the array model or the number of signal sources. Second, after network training, there are no complex operations on the input parameters, and the estimation results can be obtained by simple calculations. Third, the DL network can even extract features well in low SNR and small snapshots [21], showing good robustness and generalization ability.

The authors in [22] proposed a DNN, composed of fully connected (FC) layers for DOA estimation of two stationary targets, but high accuracy can be obtained only when  $1^\circ$  default tolerance is retained. Another DNN framework was also introduced in [23] for DOA estimation of a vector sensor. However, it mainly focused on the problem of multiple signal sources rather than improving the estimation accuracy. In [24], a DNN framework, composed of multi-task auto-encoder (AE) and multiple parallel classifiers, was proposed, where the purpose was to improve the robustness to array imperfections. While deep AE for DOA estimation with array imperfections was proposed in [25], and the influence of coherent sources was further considered. In [26], a deep convolutional neural network (CNN) for DOA estimation in low SNRs was introduced. However, it used one-dimensional convolution filter and showed limited advantages. Another CNN

was proposed in [21], where the proposed network showed a performance improvement under low SNRs. However, the resolution of DOA estimation was  $1^\circ$  and the resolution of DOA estimation was not improved. Similarly, a CNN for wide-band signal DOA estimation was proposed in [27] based on uniform circular array (UCA). The authors in [28] used a DNN to reconstruct the transmitted signal from the received signal, and MUSIC is applied to estimate DOA from the reconstructed signal. In [29] a DNN-based DOA estimation method for MIMO radar was proposed, where the authors used regression to realize grid-less DOA estimation. However, the results were tested only for on-grid signals.

DL mechanism is widely used for DOA estimation in the context of acoustic signals [30], [31], [32] as well. A convolutional recurrent neural network (CRNN) was designed in [30] to estimate DOAs of acoustic sources. The network can well estimate the DOAs of multiple sources and generate spatial pseudo-spectrum at high SNRs. However, the resolution in both azimuth and elevation is  $10^\circ$ . Grids with resolution of  $5^\circ$  were applied to obtain the position labels of the acoustic sources in [31] and [32], where a DNN [31] and a CNN [32] were proposed to estimate the DOAs of wide-band microphone array signals, respectively. The authors divided the whole DOA range with a resolution of  $5^\circ$  so as to obtain the position labels of the sound sources.

Most of the above DL-based methods have studied the adaptability of DOA estimation in different environments, that is, when the number of signal sources is unknown, under low SNRs or array imperfections. Their DOA estimation resolutions have similar upper limits, because they all adopted integer-degree-spacing signals and used large resolution grid, such as  $1^\circ$  or  $5^\circ$ , for training. Although off-grid signals are used in testing, most information in the fractional part of DOAs is actually ignored. To the best of our knowledge no specific DL-based technique was developed to achieve higher resolution DOA estimation without using more dense grids.

Considering the limitations of the aforementioned works, in this paper, we explore a simple way to achieve higher resolution of DOA estimation with a two-stage DL framework. For DL-based methods with multi-label classification (MLC) frameworks, the improvement of grid resolution means the increase of grid point number, which corresponds to the output length of the network. Then the number of the network parameters will explode greatly so that it is difficult and costly to train such a network. Inspired by the two-stage method in object detection [35], [36], [37], we design a two-stage MLP (TS-MLP) network, which divides the DOA estimation into two parts to create a finer grid with resolution of  $0.01^\circ$  for the general off-grid signal. Specifically, the covariance matrix of received signals is firstly estimated and vectorized as the input of the network, and the first stage of MLP is introduced to estimate the integer-degree portion of DOA. Afterwards, the second stage of MLP estimates the fractional-degree portion of DOA based on the concatenation of the output of the first stage and the original input. In addition, an extra label is used to pair the output of the two stages for multiple sources. Through the above process, the proposed method can attain super-resolution DOA estimation of

general off-grid signals at the lowest possible cost. Moreover, the array imperfections are analyzed and tested in detail based on the proposed network without any further adjustment. Finally, experimental results are provided to demonstrate the effectiveness and robustness of the proposed TS-MLP network.

The main contributions of this paper can be summarized as follows:

- 1) We introduce a two-stage MLP network for high-resolution DOA estimation. It divides the DOA estimation procedure into two parts, namely, integer degree and decimal degree, which are obtained by two network outputs respectively. In so doing, it can realize resolution of  $0.01^\circ$  in DOA estimation of signals without adding too many network parameters, and is different from existing DL-based methods for integer-degree DOA estimation.
- 2) We introduce a pairing method for the two-part network outputs in the presence of multiple target signals. A new tag and a new part of the network are designed to obtain pairing relationship, and the input contains the features extracted from the first two parts of the network.
- 3) Effective strategies are used to train our network. With the improvement of resolution, the angle we need to consider is no longer limited to integers, and the size of dataset increases greatly. In this study, the true covariance matrix, stepwise increased SNR pattern, and randomly selected angle pairs are used to reduce the size of the training dataset. The experimental results show that the network has the generalization ability to maintain stable performance in untrained angle pairs and low SNR conditions.

The rest of this paper is organized as follows: Section II presents the basic signal model of a linear array for DOA estimation. In Section III, we detail the data pre-processing methods and the proposed TS-MLP network. In Section IV, we discuss the training strategies of the network and the array imperfection cases. In Section V, numerous experiments are conducted to demonstrate the effectiveness and robustness of the proposed method, and Section VI concludes our work.

**Notations:** Before introducing the main body of this paper, we denote a set by Greek alphabet, e.g.,  $\chi$ , and its cardinality is  $|\chi|$ ; Matrices are denoted by boldface capital letters, e.g.,  $\mathbf{A}$ ; vectors are denoted by boldface lowercase letters, e.g.,  $\mathbf{a}$ ; and scalars are denoted by the lowercase letters, e.g.,  $a$ . The imaginary unit is  $j$  ( $j^2 = -1$ ). The transpose of a matrix is  $(\cdot)^T$  and the conjugate transpose of a matrix is  $(\cdot)^H$ .  $\mathbf{I}_N$  is the  $N \times N$  identity matrix. The symbol  $E[\cdot]$  is the expectation operator.

## II. SIGNAL MODEL

We consider the typical linear array signal model in automotive radar. Assume that  $K$  far-field narrow-band signal sources impinge on the  $N$ -element array, the received signal at time  $t$  is

$$\begin{aligned} \mathbf{y}(t) &= \sum_{k=1}^K \mathbf{a}(\theta_k) s_k(t) + \mathbf{n}(t) \\ &= \mathbf{A}(\theta) \mathbf{s}(t) + \mathbf{n}(t), \quad t = 1, \dots, L, \end{aligned} \quad (1)$$

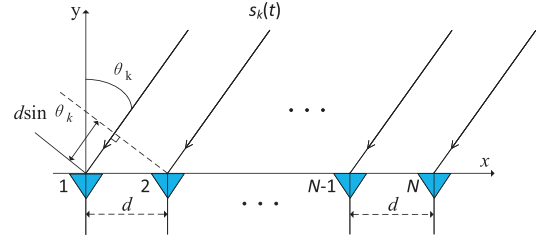


Fig. 2.  $N$ -element uniform linear array.

where  $L$  is the number of snapshots,  $\mathbf{s}(t) = [s_1(t), \dots, s_K(t)]^T \in \mathbb{C}^K$  and  $\mathbf{n}(t) \in \mathbb{C}^N$  denote the source signal and additive noise vectors, respectively. Herein,  $\mathbf{A}(\theta) = [\mathbf{a}(\theta_1), \dots, \mathbf{a}(\theta_K)] \in \mathbb{C}^{N \times K}$  is the manifold matrix, where  $\mathbf{a}(\theta_k)$  denotes the steering vector corresponding to  $\theta_k$ .

Without loss of generality, we consider the uniform linear array (ULA) model, as shown in Fig. 2. Then the steering vector can be expressed as

$$\mathbf{a}(\theta_k) = \left[ 1, e^{j \frac{2\pi d}{\lambda} \sin(\theta_k)}, \dots, e^{j \frac{2\pi (N-1)d}{\lambda} \sin(\theta_k)} \right]^T, \quad (2)$$

where  $d$  is the inter-element spacing and  $\lambda$  is the wavelength. In most cases,  $d$  is usually assumed to be half of the wavelength  $\lambda$ .

Suppose that the impinging signals are uncorrelated with each other, then the covariance matrix of signals  $\mathbf{R}_s = E[\mathbf{s}(t)\mathbf{s}^H(t)]$  is a diagonal matrix. In addition, the additive noise components are assumed to be independent identically distributed white Gaussian noise, thus the noise covariance matrix can be written as  $\mathbf{R}_n = E[\mathbf{n}(t)\mathbf{n}^H(t)] = \sigma_n^2 \mathbf{I}_N$ . Also, the signal  $\mathbf{s}(t)$  is supposed to be uncorrelated with noise  $\mathbf{n}(t)$ . Based on the above assumptions, the covariance matrix of the received signal is

$$\mathbf{R}_y \triangleq E[\mathbf{y}(t)\mathbf{y}^H(t)] = \mathbf{A}(\theta) \mathbf{R}_s \mathbf{A}^H(\theta) + \sigma_n^2 \mathbf{I}_N. \quad (3)$$

However, in practical applications, we are unable to obtain this true covariance matrix in (3). Commonly, the covariance matrix is required to be estimated with the received data of  $L$  snapshots

$$\hat{\mathbf{R}}_y = \frac{1}{L} \sum_{t=1}^L \mathbf{y}(t)\mathbf{y}^H(t). \quad (4)$$

As analyzed before, we would like to obtain the super-resolution estimation of DOAs from the received signal. However, there are only a small amount of data available and much more signal information should be explored. As an important tool to analyze the received signal, the covariance matrix is used as the input of our proposed network to extract features from received signals [38].

## III. PROPOSED TS-MLP NETWORK FOR DOA ESTIMATION

In this section, we transform the DOA estimation problem into an MLC problem. Referring to the two-stage networks on solving the object detection problem among CV tasks [35], [36], [37], we divide DOA estimation into two parts, namely, integer and decimal degrees. This method avoids sharp increase of parameters compared with directly using the finer grid. Herein,



the first part of the network is used to coarsely determine the source angle on the grid with an interval of  $1^\circ$  and the second part is to determine the decimal value using a finer grid.

#### A. Data and Label Pre-Processing

In this subsection, data and label pre-processing process is introduced. We use the  $N \times N$  covariance matrix  $\mathbf{R}_y$  of the received signal as the input of the proposed TS-MLP model. For it is a Hermitian matrix, the upper and lower parts of the main diagonal contain the same information. Therefore, we only use the covariance matrix elements of the main diagonal and the lower triangular part. However, all elements except the main diagonal are complex and cannot be directly used as the input of TS-MLP. The next step is to decompose the complex value of each element into two real values. Therefore, the input of TS-MLP network is:

$$\mathbf{x} = [\tau_{1,1}, \dots, \tau_{N,N}, \Re(\tau_{2,1}), \Im(\tau_{2,1}), \Re(\tau_{3,1}), \Im(\tau_{3,1}), \dots, \Re(\tau_{N,N-1}), \Im(\tau_{N,N-1})]^T, \quad (5)$$

where  $\tau_{i,j}, i, j \in \{1, 2, \dots, N\}$  denotes the  $(i, j)$  element of the covariance matrix,  $\Re(\cdot)$  and  $\Im(\cdot)$  denote the real and imaginary parts, respectively. The length of the input vector  $\mathbf{x}$  is  $N^2$ . Then, the total input set of the network can be viewed as a set of  $D$  vectors, defined as  $\chi = \{\mathbf{x}^1, \mathbf{x}^2, \dots, \mathbf{x}^D\}$ , where  $D$  is the total number of samples in the training set and  $\mathbf{x}^i$  represents the input vector of  $i$ -th sample.

Commonly, DOA estimation with DL networks is modeled as a MLC task, hence the output label is directly related to the DOA search range and grid spacing. Considering the DOA of each source ranged from  $\phi_{\min}$  to  $\phi_{\max}$ , and the angle resolution is  $\Delta\phi$ , then we have a grid map  $\vartheta = \{\phi_{\min}, \phi_{\min} + \Delta\phi, \dots, \phi_{\max} - \Delta\phi, \phi_{\max}\}$  with  $(\phi_{\max} - \phi_{\min})/\Delta\phi + 1$  grid points. For example, if  $\phi_{\min} = -60^\circ$  and  $\phi_{\max} = 60^\circ$ , angle resolution  $\varepsilon = 1^\circ$ , then the grid map becomes  $\vartheta = \{-60^\circ, \dots, -1^\circ, 0^\circ, 1^\circ, \dots, 60^\circ\}$ . As a result, the number of grid points, i.e., the length of the label vector becomes  $|\vartheta| = 121$  and we can acquire the  $1^\circ$  of DOA estimation results. However, if it is required to make a more accurate estimation of the common off-grid signals, it is better to make the angular resolution accurate to at least  $0.01^\circ$  corresponding to the grid map  $\vartheta = \{-60^\circ, \dots, -0.01^\circ, 0^\circ, 0.01^\circ, \dots, 60^\circ\}$ , where the set has  $|\vartheta| = 12001$  grid points. This means the length of the label vector, i.e., the number of output units of the network, will increase to 12001. In this case, the parameters of neural network will increase greatly and become hard to train.

In order to avoid numerous parameters, we borrow the concept of region proposal [35], [37] in two-stage object detection. The whole neural network is divided into two parts. The first part is used to determine the integer degree of the source DOA, i.e., to determine a candidate region of  $1^\circ$  grid. The second part fine tunes the estimate in this region, i.e., the position on the grid with a resolution  $\varepsilon = 0.01^\circ$ , as shown in Fig. 3. Therefore, the label of two parts can be determined. The first label is a  $(\phi_{\max} - \phi_{\min} + 1) \times 1$  vector  $\mathbf{z}_1$ , and it represents the integer grid with  $1^\circ$  resolution. For signal with DOA  $\theta_j$ , e.g.,  $\theta_j = 3.45^\circ$ , the label  $\mathbf{z}_1^j$  only has a non-zero value 100 at the position  $[\theta_j]_r = 3^\circ$ , where

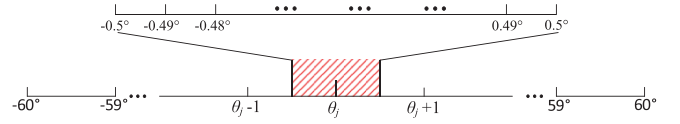


Fig. 3. Schematic diagram of label setting.

$[\cdot]_r$  denotes the round operation. Each output value is defined to express the probability [%] that the DOA angle locates at the corresponding  $1^\circ$  region after rounding. The second label is a  $100 \times 1$  vector  $\mathbf{z}_2$ , and it represents the small grid with resolution being  $0.01^\circ$  based on the region determined in the first part of the network. Note that the second label denotes both negative and positive range of the integer-degree angle estimated by the first part. For the same signal with DOA  $\theta_j = 3.45^\circ$ , the label  $\mathbf{z}_2^j$  only has a non-zero value 100 at the position  $(\theta_j - [\theta_j]_r)/0.01 + 50$ .

#### B. Two Network Output Pairing

Through the previous data processing and label setting, more accurate DOA estimation can be achieved than the previous DL-based methods. However, when there are multiple targets, the correspondence between the outputs needs to be determined. Therefore, a third label is designed to indicate the corresponding relationship between the peaks of the probability spectrum of the two outputs.

For  $K$  far-field narrow-band signals, there are  $K!$  different combinations, and a vector with length  $K!$  is needed to represent all corresponding relationships between integer and decimal parts. Regarding to automotive radars studied in this paper, DOAs are usually estimated for the potential targets in the same range-velocity bin. Actually, existing automotive radars can already achieve very high range and velocity resolutions, so there are few situations where DOA estimation is required for three or more targets. It can be considered that the number of possible targets within the same range-velocity bin is always small and less than or equal to two. Therefore, the complexity of such pairing setting is acceptable. So in this paper, considering there are two sources with different angles, two possible relationships between the two network outputs are required to pair two sources. Then the pairing label is defined as

$$\mathbf{z}_3 = \begin{cases} [1, 0]^T & \text{Situation 1} \\ [0, 1]^T & \text{Situation 2,} \end{cases} \quad (6)$$

where “Situation 1” denotes the situation that the larger integer part corresponds to the larger decimal part and “Situation 2” is the opposite. Hence, the  $j$ -th training sample consists of pairs in the form  $(\mathbf{x}^j, \mathbf{z}_1^j, \mathbf{z}_2^j, \mathbf{z}_3^j)$ , including one input sample and three labels, leading to the training data set  $\kappa_{train} = \{(\mathbf{x}^1, \mathbf{z}_1^1, \mathbf{z}_2^1, \mathbf{z}_3^1), (\mathbf{x}^2, \mathbf{z}_1^2, \mathbf{z}_2^2, \mathbf{z}_3^2), \dots, (\mathbf{x}^D, \mathbf{z}_1^D, \mathbf{z}_2^D, \mathbf{z}_3^D)\}$ . Although the complexity of this pairing scheme may be very high when the number of targets is large, DOA estimation is usually carried out for targets in the same distance-velocity bin, and the number of such targets is not large, in most cases it is two. In Section V, we simulate multiple different cases to demonstrate that the proposed pair label is able to distinguish two sources.

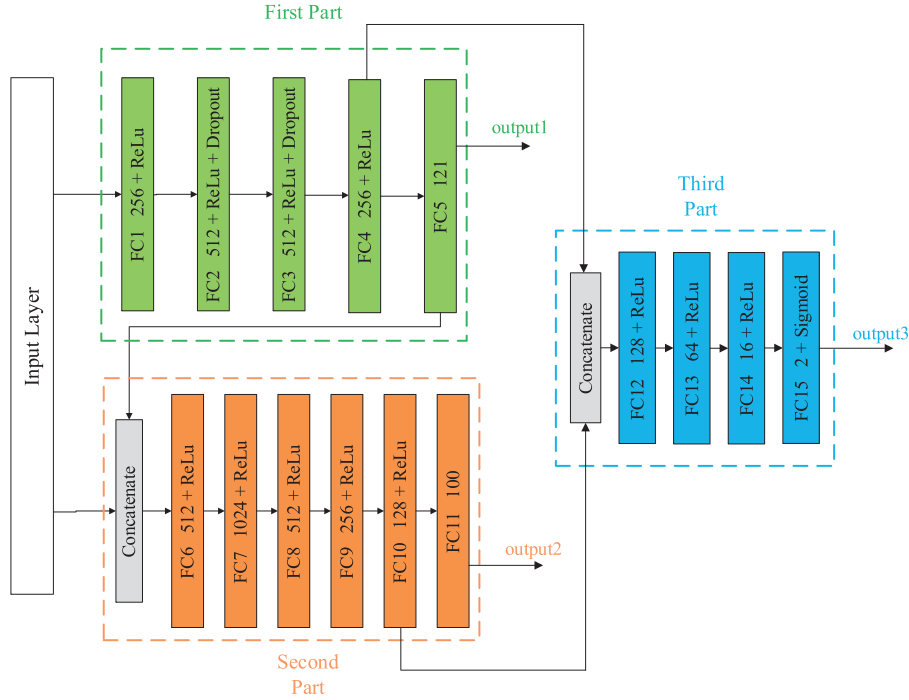


Fig. 4. Architecture of the proposed TS-MLP for super-resolution DOA estimation. The network consists of full connection (FC) layers with *ReLU* activation function, except for the three output layers. The output layers of the first and second parts use identity function, and the output layer of the third part uses the *Sigmoid* activation function. The input of the first part is the original input of the network, the input of the second part is the combination of the original input of the network and the output of the first part, and the input of the third part is the combination of the features extracted by the first two parts of the network. Two dropout layers are employed (for regularization) to the first part of the network.

### C. Proposed TS-MLP Architecture

In this subsection, the proposed network is specifically introduced. Basically, neural network can adjust the relationship between a large number of internal nodes, realize the nonlinear mapping from input to output. The universal approximation theorem indicates that a single-layer feedforward neural network with enough neurons can approximate any continuous function on a compact subset of  $\mathbb{R}^n$  [39]. In practical applications, MLP with finite neurons are usually used to approximate the mapping relationship between inputs and required outputs. After using back propagation (BP) algorithm [40], the MLP can learn or adjust the parameters in the mapping process to better approximate the desired results. In addition, activation functions are always used in the network to realize nonlinear transformation.

As we analyzed before, the proposed network has one input and three outputs. The input is a vector of length  $N^2$  and the outputs are vectors of lengths 121, 100, and  $K!$ , respectively, corresponding to the integer part, the decimal part, and the pairing label part. The overall structure of the network is inspired by the idea of two-stage target detection, such as region with CNN features (R-CNN) [35], as shown in Fig. 4. In the first part, the grid spacing is  $1^\circ$ , which plays a role in determining the candidate grid region. Then the second part divides the grid points with an interval of  $0.01^\circ$  in the region near the grid points determined in the first part, realizing a higher resolution. The last part of the network determines the corresponding relationship between the outputs of the above two parts when considering the case of multiple sources. The inputs of the second and third

parts can be expressed as:

$$\mathbf{x}_2 = \text{concatenate}(\mathbf{x}_1, \mathbf{y}_1), \quad (7)$$

$$\mathbf{x}_3 = \text{concatenate}(f_1(f_2(\dots f_4(\mathbf{x}_1))), f_6(f_7(\dots f_{10}(\mathbf{x}_2))). \quad (8)$$

where  $\mathbf{x}_1, \mathbf{x}_2$  and  $\mathbf{x}_3$  represent the inputs of the three parts,  $\mathbf{y}_1$  represents the output of first part, and each  $\{f_i(\cdot)\}_{i=1,\dots,15}$  denotes a dense layer.

Among these dense layers, the output layer  $f_5(\cdot)$  and  $f_{11}(\cdot)$  have no activation function, and  $f_{15}(\cdot)$  uses the *Sigmoid* activation function  $f_{\text{Sigmoid}}(u) = 1/(1 + e^{-u})$  to map the input to values between  $[0,1]$ , and other layers use the *ReLU* activation function  $f_{\text{ReLU}}(u) = \max(u, 0)$ .

For the output vectors  $\mathbf{z}_1$  and  $\mathbf{z}_2$ , the location of the peak values represent the integer region and decimal angle of the estimated DOAs, respectively. The value of  $\mathbf{z}_3$  is  $[1,0]$  or  $[0,1]$ , which represents the corresponding relationships of both two-stage outputs. Moreover, in the process of network training, we found that the convergence speed of the first part of the network is significantly faster than that of the second part, and over-fitting can easily occur. Therefore, we added dropout layers after the dense layers  $f_2(\cdot)$  and  $f_3(\cdot)$  in the first part of the network to avoid this situation. The dropout layers randomly set weights to zero with probability 50% (untrainable parameters) and act as regularization to the learning process. The layout of the proposed TS-MLP is depicted in Fig. 4.

TS-MLP is trained in a supervised way on dataset  $\kappa_{train}$ . The parameters of the network are continuously optimized and adjusted via BP algorithm by minimizing the reconstruction error. The first two parts of the network use the mean square error (MSE) to construct the loss function

$$L_{MSE} = \frac{1}{J} \sum_{j=1}^J (y_j - z_j)^2, \quad (9)$$

where  $J$  is the output size,  $y_j$  and  $z_j$  represent the  $j$ -th element of the network output and the true label, respectively. For the first and second parts of the network, the values of  $J$  are 121 and 100, respectively. And the third part uses the binary cross-entropy as the loss function

$$L_{binarycross-entropy} = -\frac{1}{J} \sum_{j=1}^J [z_j \cdot \log y_j + (1 - z_j) \log(1 - y_j)], \quad (10)$$

where  $J = 2$ . Till now, all the preparation before network training, including the data pre-processing, two-stage output pairing, and network architecture are described. In the next section, we will present the training approach and array imperfection cases in detail.

#### IV. DOA ESTIMATION WITH TS-MLP

##### A. Training Approach

In order to train the proposed TS-MLP network, we set  $\phi_{\min} = -60^\circ$  and  $\phi_{\max} = 60^\circ$ . The first two parts of the network output  $1^\circ$  and  $0.01^\circ$  resolution grids, respectively. Considering two source signals, the output vector dimensions of the three parts in the TS-MLP network are 121, 100, and 2.

Since the angle resolution is increased to  $0.01^\circ$ , the amount of data, required for training, is greatly increased. Therefore, we take several measures to reduce the number of training samples: i) The angular interval between two sources is smaller than  $10^\circ$ , that is to say, we only consider the situation for closely located sources ( $1^\circ \leq \Delta\theta < 10^\circ$ ). Another reason for using this method is that in the DOA estimation problem, we usually pay more attention to the estimation results when the target angles are relatively close. ii) Referring to the training method in [21], we generate the input data from the true covariance matrix in (3) for training the network and use the sample covariance in (4) for testing and evaluation. For a single angle pair, we use the true value to represent all other possible estimates, so that the input data number is greatly decreased.

Next, we describe the generation method of the training dataset. As mentioned before, we consider the number of signal sources  $K = 2$ , so there are more than 70 million kinds of different DOA pairs in total. Even if we only consider the situation for closely separated angles as aforementioned, the total number of combinations will also reach 10,306,350, which is still too large. Hence, for each angle interval  $\Delta\theta \in [1^\circ, 1.01^\circ, \dots, 9.99^\circ]$ , we randomly generate 5,000 pairs of angles, and obtain 4,500,000 training examples per SNR value. When training the proposed TS-MLP network for different SNR conditions, we used the

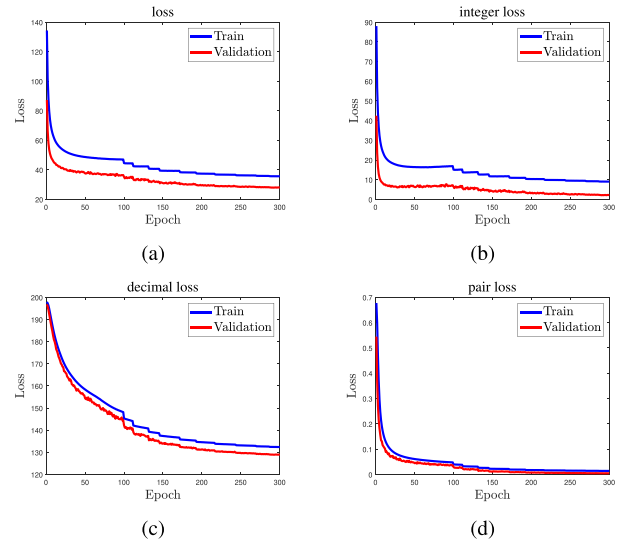


Fig. 5. Training and validation losses of the TS-MLP for each training epoch: (a) global network loss; (b) first part of the network representing the integer part; (c) second part of the network representing the decimal part; (d) third part of the network representing the pairing relationship.

input data from different SNRs, such as  $\{0, 5, 10, 15, 20, 25, 30\}$  dB. Then the number of training samples increases to  $D = 7 \cdot 4,500,000 = 31,500,000$  in total. One reason for choosing such a SNR pattern is that it can also reduce the size of the dataset since it does not include the negative region of SNR. On the other hand, the DL-based method demonstrates good tolerance for data imperfections, hence it shows robust performance even in the case of untrained SNR. In addition, in previous research works, it is found that increasing the conditions of training SNRs can only slightly improve the performance.

During the TS-MLP training, the dataset is randomly divided into training set (90%) and verification set (10%). The network was trained for 300 epochs with mini-batch size of 1,000. In Fig. 5(a), we plot total network loss of training and validation at each epoch. Moreover, Fig. 5(b), (c), and (d) show the loss of three parts of the network. It can be observed that the validation loss is always lower than the training loss, hence there is no overfitting problem. The initial learning rate is set to 0.0001, and the parameters are optimized by the adaptive moment estimation [41]. In addition, when the validation loss reached plateau for 10 epochs, the learning rate decays by a factor of 0.7. The loss weights of the three outputs were set to 1, 0.2, and 10, respectively. Compared with the decimal part output, we pay more attention to the accuracy of the integer part, i.e., the determined candidate region. The third output uses the cross-entropy loss function, so it is necessary to increase the loss weight. The network was implemented in Keras using Tensorflow as the backend. The experiment platform is Ubuntu running on a server with an NVIDIA GeForce RTX 3090 GPU.

##### B. Computational Complexity

For DL-based DOA estimation methods, the main complexity is in the training stage. After the model is well trained, the actual estimation is carried out with very simple operations,

TABLE I  
MODEL COMPLEXITY AND AVERAGED COMPUTING TIME

	TS-MLP	MUSIC	RMUSIC	ESPRIT	NN	CNN
		[3]	[4]	[5]	[19]	[18]
Total params	1,985,103	/	/	/	107,971	15,609,721
Test time /s	3.06e <sup>-4</sup>	5.70e <sup>-1</sup>	8.74e <sup>-4</sup>	4.61e <sup>-4</sup>	6.74e <sup>-5</sup>	4.36e <sup>-4</sup>

which takes less time than traditional methods and is more suitable for systems with limited computing power. In Table I, we compare the calculation time of various DOA estimation methods and show the number of model parameters of each DL-based method. Each method performs 1,000 operations on the same equipment and the time for single estimation is obtained after averaging.

It can be seen from the table that the running times of DL-based methods are generally less than those of the traditional methods. Although TS-MLP uses a two-stage structure and contains many parameters to obtain more accurate DOA estimation results, it can still meet the real-time requirements. It is worth noting that this test is carried out on a high-performance personal computer. If it is on a platform with limited computing power, the advantages of DL-based methods will be obvious because traditional subspace-based methods usually involve complicated operations such as matrix inversion. In addition, neural networks can be implemented by analog circuits, and processing time can reach the nanosecond level [19].

### C. Array Imperfection Analysis

Array imperfection problem is one of the common problems in DOA estimation, and has received extensive attention for the past decades [24], [25], [42], [43], [44], [45], [46], [47]. There are three typical kinds of array imperfection: a) gain and phase error ( $e_g$  and  $e_p$ ) [42], [43], [44], b) mutual coupling error ( $e_{mc}$ ) [45], [46], and array element position error ( $e_{ps}$ ) [42], [47]. In this paper, we use a simplified model to simulate and test the stability of the proposed model under all three kinds of array imperfection [24]. The gain biases of the array sensors are

$$e_g = \rho \times [g_1, g_2, \dots, g_N]^T, \quad (11)$$

where  $g_n$  is a random number between  $[-1, 1]$ , and the parameter  $\rho \in [0, 1]$  is used to control the strength of the imperfection. The phase biases are

$$e_p = \rho \times [p_1, p_2, \dots, p_N]^T, \quad (12)$$

where  $p_n$  is a random number between  $[-10^\circ, 10^\circ]$ . The mutual coupling coefficient vector is

$$e_{mc} = \rho \times [0, \gamma^1, \dots, \gamma^{N-1}]^T, \quad (13)$$

where  $\gamma = 0.2e^{j20^\circ}$  is the mutual coupling coefficient between adjacent array elements.

The position biases are

$$e_{ps} = \rho \times [pos_1, pos_2, \dots, pos_N]^T \times d, \quad (14)$$

where  $pos_n$  is a random number between  $[-1, 1]$ .

By adjusting the coefficient  $\rho$ , the array imperfections with different strengths can be produced, and the array steering vector

$\mathbf{a}(\theta_k)$  in (1) is rewritten as:

$$\begin{aligned} \mathbf{a}(\theta, \mathbf{e}) &= (\mathbf{I}_N + \delta_{mc} \mathbf{E}_{mc}) \times (\mathbf{I}_N + \text{Diag}(\delta_g \mathbf{e}_g)) \\ &\times \text{Diag}(\exp(j\delta_p \mathbf{e}_p)) \times \mathbf{a}(\theta, \delta_{ps} \mathbf{e}_{ps}), \end{aligned} \quad (15)$$

where  $\delta_{(\cdot)}$  is used to indicate whether a certain kind of imperfection exists,  $\text{Diag}(\cdot)$  forms diagonal matrices with the given vector on the diagonal and  $\mathbf{E}_{mc}$  is defined as a Toeplitz matrix with parameter vector  $\mathbf{e}_{mc}$ .

## V. EXPERIMENTAL RESULTS

This section carries out simulations to show the super-resolution DOA estimation performance of the proposed TS-MLP network. First, we show how the whole network works through specific inputs. Second, we evaluate the performance of the network under various settings. Third, we analyze the statistical performance of the network. Finally, we test the stability of the network in the case of array imperfections.

In both training and testing phases, we consider a ULA with  $N = 12$  elements. In order to show the super-resolution DOA estimation characteristics of the proposed model, we compare the simulation results with traditional and DL methods: 1) MUSIC [3]; 2) RMUSIC [4]; 3) ESPRIT [5], [6]; 4) DNN [22]; 5) CNN [21]. Among these methods, 1-3) are traditional DOA estimation methods, and 4-5) are DL-based DOA estimation methods. For the on-grid methods, like MUSIC, the grid resolution is chosen to be the same as that of the proposed method, i.e.,  $\varepsilon = 0.01^\circ$ . Furthermore, in order to ensure the consistency of the comparison conditions, we also used the same SNRs with stepwise growth in the dataset of the DL-based methods 4-5). Also, we adjusted the dataset in 4) to consider all angle pairs, rather than random generation. Note that we mainly consider the ability to estimate the DOAs of two sources, since it is to unify the experimental conditions with other researches and it is the most common situation in practice.

### A. DOA Estimation of Specific Inputs

In the first group of experiments, we the proposed TS-MLP network through specific inputs to demonstrate its working mechanism and superior performance. In the first experiment, two narrow-band signals from directions of  $-20.17^\circ$  and  $-15.63^\circ$  impinge on the array with the SNR being 20 dB, and the outputs of the first two parts are shown in Fig. 6(a)–(b). We consider that  $L = 1,000$  snapshots are collected to calculate the covariance matrix according to (4). The peak locations in Fig. 6(a) are  $-20^\circ$  and  $-16^\circ$  while the peak locations in Fig. 6(b) are  $-0.18^\circ$  and  $0.39^\circ$ , and the third output is  $[1, 0]^T$ . Consequently, the estimated results of the network are  $-20.18^\circ$  and  $-15.61^\circ$ . The DOAs of two signals are well estimated with a very high accuracy.

In the second experiment, two signals located in  $10.42^\circ$  and  $13.75^\circ$  are considered when  $\text{SNR} = 0$  dB, the outputs of the first two parts of the network are shown in Fig. 6(c) and (d). As can be seen, the integer parts of DOAs in Fig. 6(c) are  $10^\circ$  and  $14^\circ$ , and meanwhile, the decimal parts of DOAs in Fig. 6(d) are  $-0.28^\circ$  and  $0.38^\circ$ . The third output is  $[0, 1]^T$ , hence the estimated result



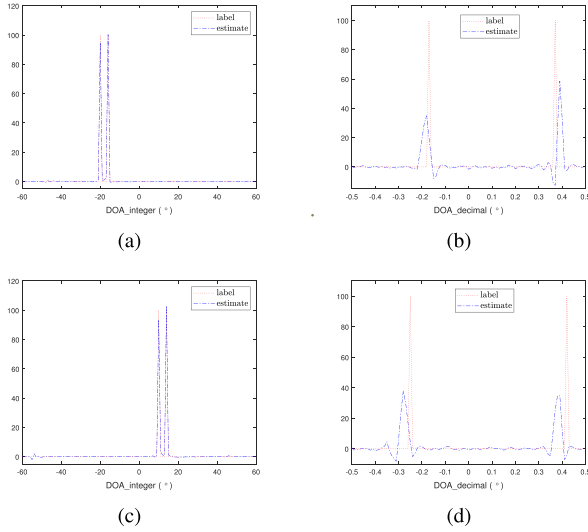


Fig. 6. Network outputs of two signals. First row:  $-20.17^\circ$  and  $-15.63^\circ$  at SNR = 20 dB. Second row:  $10.42^\circ$  and  $13.75^\circ$  at SNR = 0 dB. (a) and (c) output of first part of network, (b) and (d) output of second part of network.

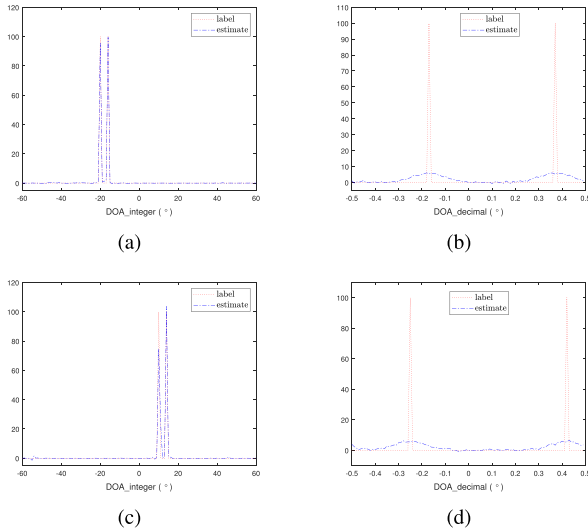


Fig. 7. Network outputs averaged by 10,000 times of two signals. First row:  $-20.17^\circ$  and  $-15.63^\circ$  at SNR = 20 dB. Second row:  $10.42^\circ$  and  $13.75^\circ$  at SNR = 0 dB. (a) and (c) output of first part of network, (b) and (d) output of second part of network.

of the network is  $10.38^\circ$  and  $13.72^\circ$ . Therefore, TS-MLP can accurately estimate the probability spectrum of signal DOAs on the predetermined rough grid, and on this basis, use a finer grid to estimate the off-grid part. Combined with the corresponding relationship given by the output of the third part, we can obtain the super-resolution estimation of DOA, which is also effective in the case of low SNRs.

It is worth mentioning that the above experiment is to illustrate the working mode of the proposed TS-MLP network, and Fig. 6 shows the result of one single test. To further illustrate its stability, we repeated the same experiment 10,000 times and the average DOA estimates are depicted in Fig. 7. Herein, the proposed TS-MLP can stably and accurately estimate the candidate

regions, that is, the integer part of DOAs. While estimation of the fractional part is always distributed near the true value with small deviations. Due to the difficulty in achieving 100% accuracy in estimating the off-grid part, there may be slight deviations in each estimation, resulting in less obvious peak spectra after averaging. In Fig. 7(b), the two peaks are located at  $-0.18^\circ$  and  $0.36^\circ$ . While in Fig. 7(d), the two peaks are located at  $-0.28^\circ$  and  $0.43^\circ$ .

### B. Further Experiments Compared With SOTA Methods

In the second series of experiments, we fix the angle interval of two sources and change DOAs in a regular step. First, the direction  $\theta_1$  of the first source varies from  $-59.67^\circ$  to  $57.33^\circ$  with an increasing step of  $1^\circ$ . Then the angle-interval  $\Delta\theta$  between two sources is fixed to  $1.8^\circ$  and  $L = 500$  snapshots are used to estimate the covariance matrix at SNR = 10 dB. The DOAs predicted by the proposed TS-MLP are shown in Fig. 8(a) where the solid lines denote the true DOAs and the corresponding errors are illustrated in Fig. 8(g). Moreover, the DOA estimates of the MUSIC method, the RMUSIC method, the ESPRIT method, the DNN method, and CNN method are shown in Fig. 8(b)–(f), respectively, and the corresponding errors are shown in Fig. 8(h)–(l) for further comparison.

Despite the small angle interval between two targets, it is noted that the errors of the proposed TS-MLP are within the range  $[-0.31^\circ, 0.6^\circ]$  for all tested samples. Except for several individual outliers, the DOA estimation errors in most cases are within a quite small range  $[-0.15^\circ, 0.15^\circ]$ . Regarding to the other two DL methods, they ignore the information of the decimal part. Furthermore, CNN performs better than DNN and its DOA estimation errors are in the range  $[-0.67^\circ, 0.33^\circ]$ . On the other hand, among the traditional DOA estimation methods, MUSIC shows large estimation errors at the boundary of the angle region, and the errors of RMUSIC and ESPRIT increase as well. From this point of view, the TS-MLP shows better robustness and it beats other methods.

Second, we consider varying  $\theta_1$  from  $-49.4^\circ$  to  $45.6^\circ$  and  $\theta_2$  from  $-45.4^\circ$  to  $49.6^\circ$  with the same step of  $1^\circ$ , i.e., the angle interval is fixed to  $4^\circ$ . Herein, the SNR is 20 dB and the covariance matrix is estimated via  $L = 2,000$  snapshots. The DOA estimates of the proposed TS-MLP, MUSIC, RMUSIC, ESPRIT, DNN, and CNN are depicted in Fig. 9(a)–(f), and their corresponding errors in Fig. 9(g)–(l), respectively.

It can be observed that the performance of the proposed TS-MLP is remarkable, where the errors are almost kept within  $0.1^\circ$  for all tested samples and is close to those of the three traditional methods. On the contrary, the other two DL-based methods have relatively large errors because the DOAs are only estimated on a rough grid. For data-driven DL-based methods, it is likely that the estimation results may fluctuate on certain samples due to the training data and process. For example, NN shows errors greater than  $1^\circ$  on some test samples, while TS-MLP and CNN perform well in this regard. There are no errors in estimates based on  $1^\circ$  grids, and TS-MLP achieved further improvement in accuracy. This indicates that achieving finer grid through multiple outputs and improving the resolution of DOA estimation is effective.



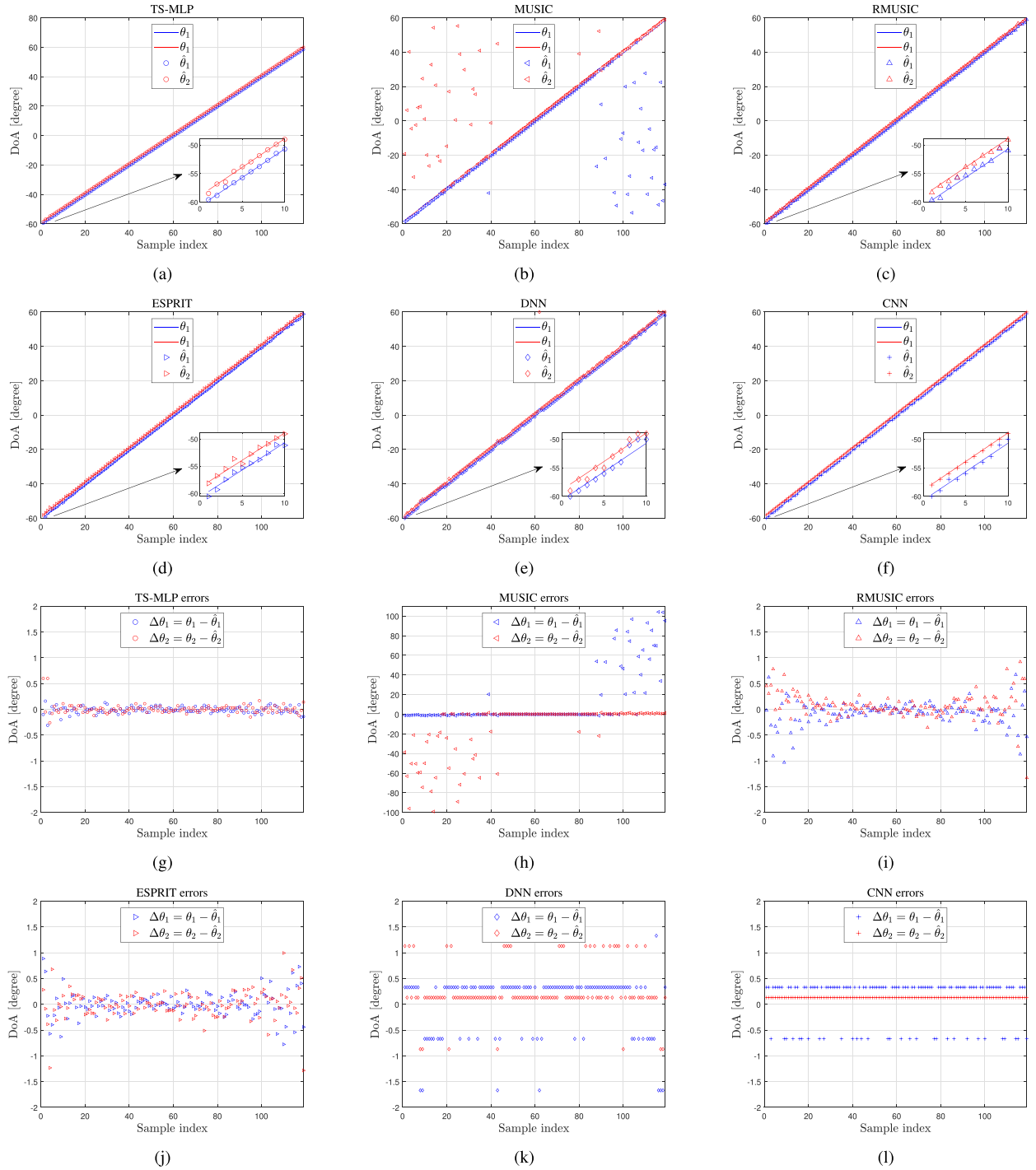


Fig. 8. DOA estimation performance on angles  $\theta_1, \theta_2 \in [-60^\circ, 60^\circ]$  with an interval of  $1^\circ$  at 10 dB SNR using  $L = 500$  snapshots. DOA estimates: (a) TS-MLP (proposed), (b) MUSIC, (c) RMUSIC, (d) ESPRIT, (e) DNN and (f) CNN. The DOA estimation errors of the: (g) TS-MLP, (h) MUSIC, (i) RMUSIC, (j) ESPRIT, (k) DNN and (l) CNN.

Then, we consider two signals with fixed angular spacing  $\Delta\theta = 2.66^\circ$  impinging onto the array. The angle of the first signal increases in step of  $0.1^\circ$  from  $-20^\circ$  to  $17^\circ$ . The covariance matrix is estimated with  $L = 1,000$  snapshots and  $\text{SNR} = 20$  dB. The DOAs estimated by the proposed TS-MLP are depicted in Fig. 10(a), whereas in Fig. 10(g) the corresponding errors are plotted. Additionally, in Fig. 10(b), (c), and (e), we show the DOA estimation results of MUSIC, RMUSIC and DNN,

respectively. ESPRIT's and CNN's DOA estimates are depicted in Fig. 10(d) and (f) and with their errors in Fig. 10(h) and (i), respectively. Here, only the errors of ESPRIT method are revealed for the performance of the three traditional methods is almost the same.

We observe that the proposed TS-MLP errors lie in the interval  $[-0.69^\circ, 0.61^\circ]$ . Furthermore, in most cases the errors lie in the interval  $[-0.1^\circ, 0.1^\circ]$ , which can compete with ESPRIT method.

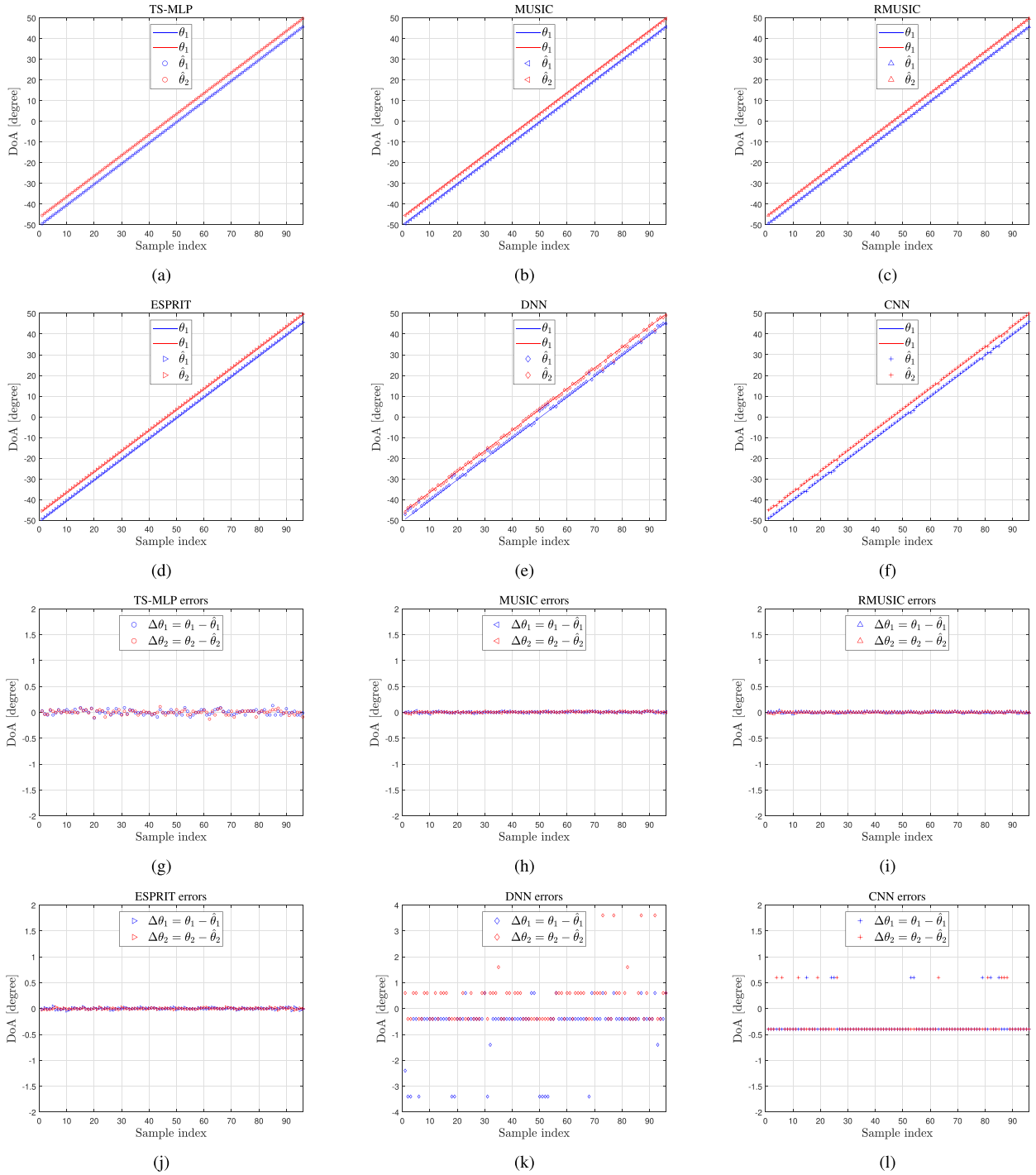


Fig. 9. DOA estimation performance on angles  $\theta_1, \theta_2 \in [-50^\circ, 50^\circ]$  with an interval of  $4^\circ$  at 20 dB SNR using  $L = 2,000$  snapshots. DOA estimates: (a) TS-MLP (proposed), (b) MUSIC, (c) RMUSIC, (d) ESPRIT, (e) DNN and (f) CNN. DOA estimation errors of: (g) TS-MLP, (h) MUSIC, (i) RMUSIC, (j) ESPRIT, (k) DNN and (l) CNN.

On the other hand, the errors of the CNN method [21] mostly lie in the interval  $[-0.8^\circ, 0.66^\circ]$  which outperforms DNN. As can be clearly seen in Fig. 10(e)–(f), the estimates of two DL-based methods rise with a  $1^\circ$  step in this setup. For the three traditional methods, their DOA estimation performance in the test interval, i.e.,  $\{-20^\circ, 20^\circ\}$ , is almost the same. In addition, the proposed TS-MLP method does not achieve the desired performance in 12 of the 370 testing samples, but the errors are still controlled

within  $\pm 0.7^\circ$ . The fluctuation of TS-MLP on a few test samples is likely due to the training samples. For simplification, the angle combinations in the training set are less than half of all possible scenarios and are randomly selected. Although neural networks can effectively compensate for such data gaps, in this experiment, with a large number of test samples and small step width, fluctuations are more likely to occur. For TS-MLP, the number of samples with fluctuations is very small and the

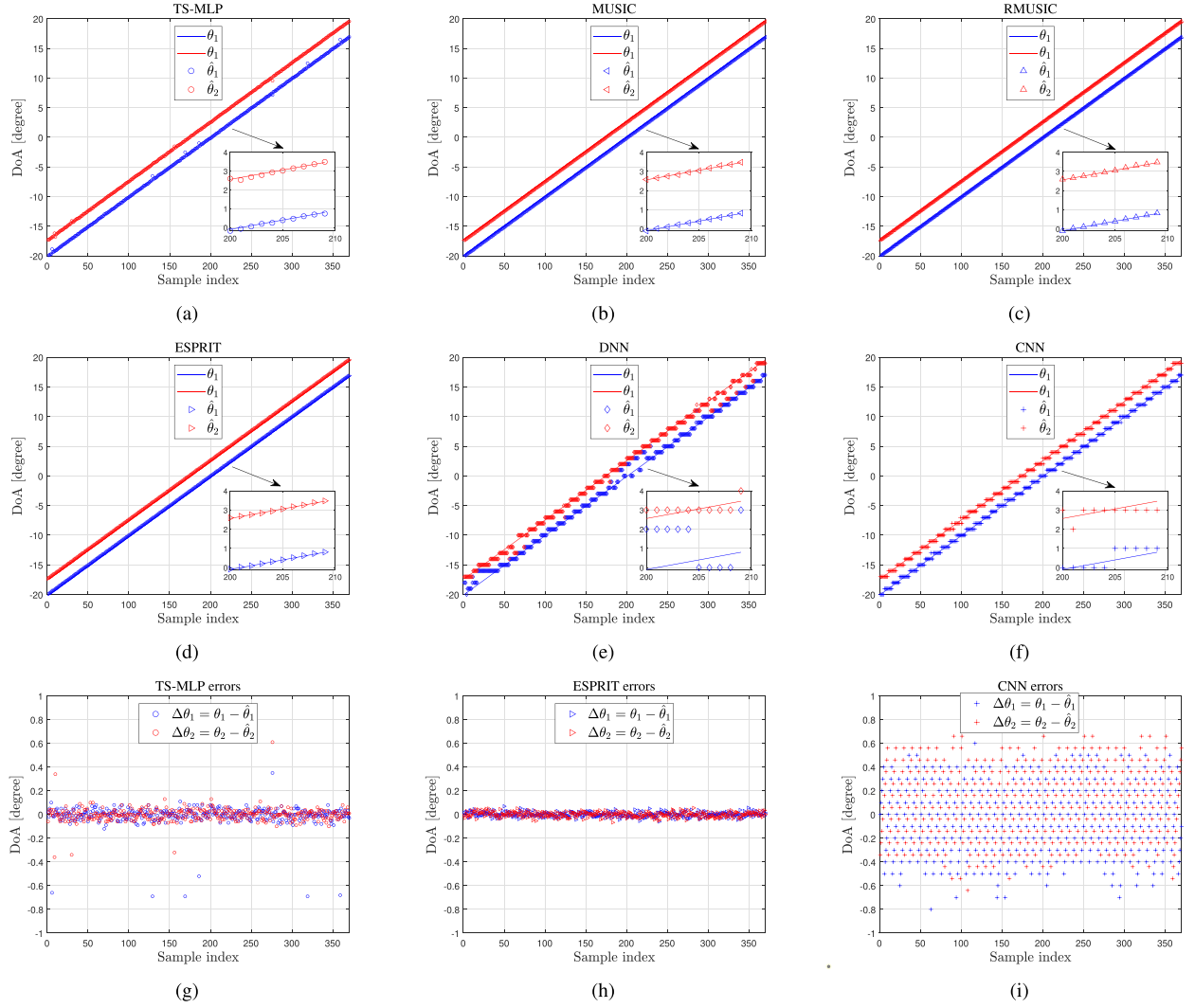


Fig. 10. DOA estimation performance on angles  $\theta_1, \theta_2 \in [-20^\circ, 20^\circ]$  vary by  $0.1^\circ$  at 20 dB SNR using  $L = 1,000$  snapshots. Results of: (a) TS-MLP (proposed), (b) MUSIC, (c) RMUSIC, (d) ESPRIT, (e) DNN and (f) CNN. DOA estimation errors of: (g) TS-MLP, (h) ESPRIT and (i) CNN.

errors are negligible, indicating a significant improvement in accuracy compared to CNN. In general, TS-MLP has achieved the expected effect, and its overall performance is far better than other DL-based methods.

Next, the angle increasing step is set to the resolution of our proposed network, i.e., the DOAs change by  $0.01^\circ$  each time. The direction of the first signal varies from  $-1^\circ$  to  $0^\circ$ , and the angular interval is set to  $1.75^\circ$ . In this case,  $L = 2,000$  snapshots are collected for estimation while SNR = 13 dB. The DOA estimates are shown in Fig. 11. The result of DNN is not included because it fails to estimate the results at several sample points for the small angular interval.

Although the tested SNR setting is not included in the training set, the performance of TS-MLP remains stable. We can notice that the errors of TS-MLP are kept within  $\pm 0.1^\circ$ , which are similar to or even better than those of the MUSIC, RMUSIC, and ESPRIT, for almost all sample points. The maximum positive and negative errors of TS-MLP are  $0.15^\circ$  and  $-0.24^\circ$  in

Fig. 11(f). However, the CNN method with  $1^\circ$  resolution shows no useful response when the target angles change with a smaller step width and presents serious performance deficiencies. So to speak, the proposed TS-MLP method demonstrates significant performance improvement in DOA estimation.

### C. Statistical Performance

In the third experiment, we use the average root-mean-square-error (RMSE) to evaluate the statistical performance of all methods. The RMSE is defined as:

$$\text{RMSE} = \sqrt{\frac{1}{KM} \sum_{k=1}^K \sum_{m=1}^M \left( \hat{\theta}_k^{(m)} - \theta_k^{(m)} \right)^2}, \quad (16)$$

where  $K$  is the number of sources and  $M$  is the total number of testing examples. Herein,  $[\hat{\theta}_1^{(m)}, \dots, \hat{\theta}_K^{(m)}]^T$  and  $[\theta_1^{(m)}, \dots, \theta_K^{(m)}]^T$  are the estimated and true DOAs of the  $m$ -th

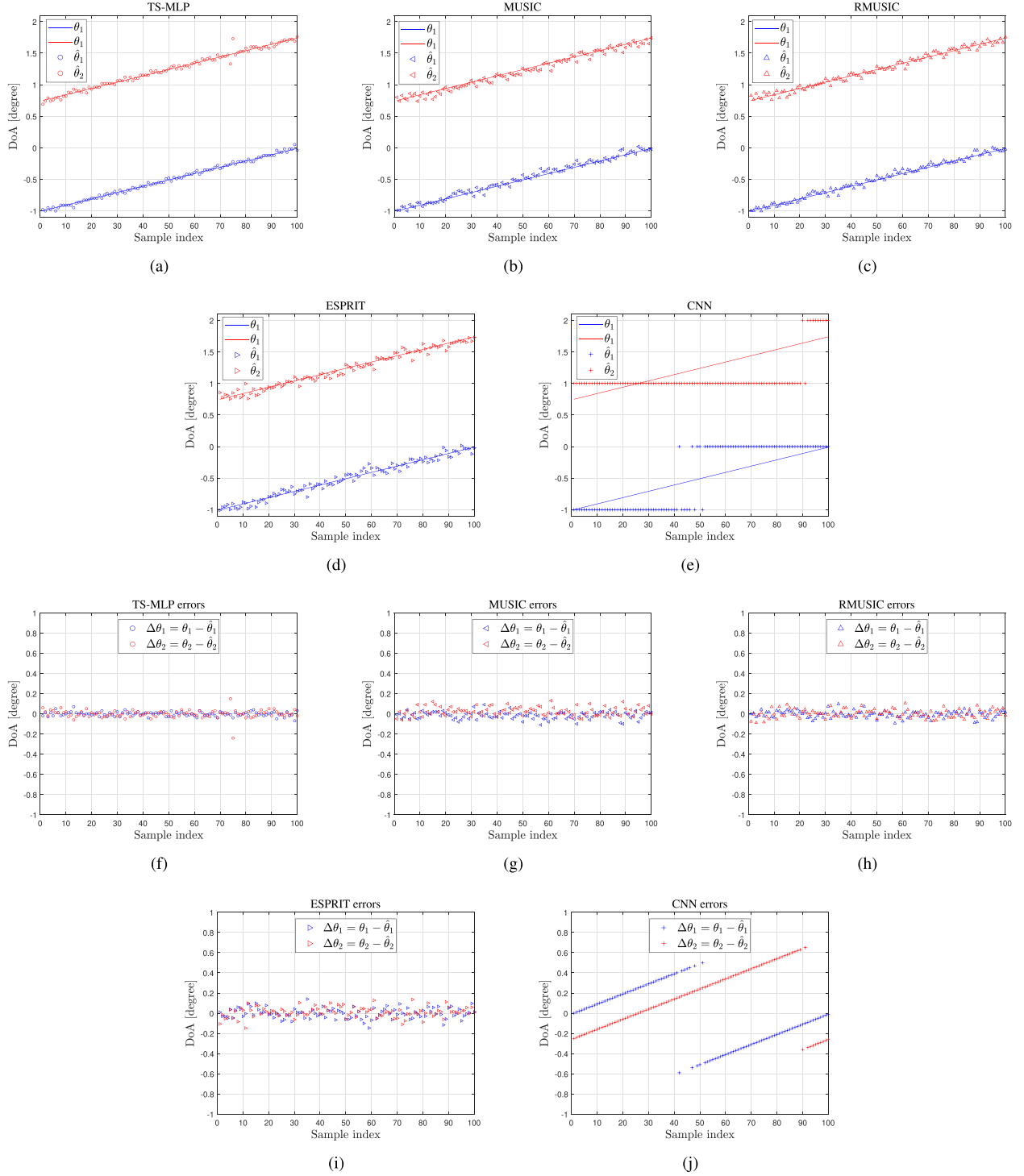


Fig. 11. DOA estimation performance on angles  $\theta_1, \theta_2 \in [-1^\circ, 1.75^\circ]$  vary by  $0.01^\circ$  when SNR = 13 dB using  $L = 2,000$  snapshots. Results of: (a) TS-MLP (proposed), (b) MUSIC, (c) RMUSIC, (d) ESPRIT, and (e) CNN. DOA estimation errors of: (f) TS-MLP, (g) MUSIC, (h) RMUSIC, (i) ESPRIT, and (j) CNN.

testing sample, respectively. Three basic experiments are given in this subsection and comparison to the Cramér-Rao lower bound (CRLB) [7] is provided.

1) *RMSE Versus SNR*: First, two signals, located at the directions  $16.37^\circ$  and  $19.15^\circ$ , are considered while the SNR

conditions are  $[-10, -5, 0, 5, 10, 15, 20, 25, 30]$  dB. At each SNR level, the RMSE is calculated over  $M = 1,000$  independent simulations and the sample covariance matrix is estimated by using  $L = 1,000$  snapshots. Then the RMSE versus SNR is plotted in Fig. 12. As can be seen, within the whole SNR



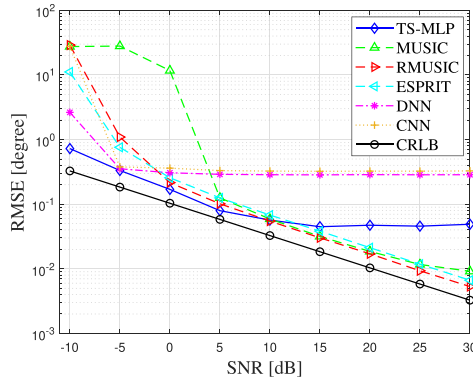


Fig. 12. RMSE versus SNR in DOA estimation of two sources using  $L = 1,000$  snapshots.

range, the TS-MLP performs better than the other two DL-based methods and its RMSE drops below 0.1 in the high-SNR region. Although the proposed method achieves finer grid by using multiple outputs, but the limitations brought by the grid still exist. Therefore, when the SNR is increased to a certain extent, RMSE does not decrease. But compared to the other two DL based methods, there has been a significant improvement and can meet the application requirements in most cases. In addition, compared with some traditional grid-less methods, like RMUSIC and ESPRIT, TS-MLP takes a quite short period for DOA estimation, which is a great advantage in practical applications. Moreover, in the low-SNR region, like  $\text{SNR} < 10$  dB, the proposed TS-MLP method outperforms the traditional grid-less methods. The results also indicate that the RMSE drops to a flat level for all grid-based methods, including the MUSIC method, in the high-SNR regime. The resolution of MUSIC taken in this experiment is  $0.01^\circ$ , so it has a higher upper limit of accuracy. Only grid-less estimators, RMUSIC and ESPRIT can continuously approach the CRLB performance.

2) *RMSE Versus Angular Interval  $\Delta\theta$* : Second, we evaluate the performance of the proposed TS-MLP method for estimating DOAs of two sources with various angular interval  $\Delta\theta \geq 1^\circ$ . Herein, the SNR is set as 15 dB. The direction of the first target is fixed to  $\theta_1 = -13.64^\circ$  and the direction of the second target is  $\theta_2 = \theta_1 + \Delta\theta$ , while the value of  $\Delta\theta$  is within the set  $\{1^\circ, 1.2^\circ, 1.5^\circ, 2^\circ, 4^\circ, 6^\circ, 8^\circ\}$ . For each  $\Delta\theta$  the RMSE is averaged over 1,000 independent tests and the covariance matrix is estimated by 1,000 snapshots. Then RMSE curve versus angular interval is illustrated in Fig. 13. As can be seen, the TS-MLP outperforms the other two  $1^\circ$ -resolution DL-based methods in all test angular intervals, because TS-MLP achieves an effect equivalent to a finer grid by using multiple outputs. In addition, the performance of TS-MLP will not deteriorate under smaller angular spacing. On the contrary, it has unique advantages for closely separated angles ( $1^\circ \leq \Delta\theta \leq 2^\circ$ ). One can also observe that the effects of DL-based methods are almost constant for all angle intervals, this may be due to their data-driven characteristics. The change of angle interval does not affect the difficulty of information extraction as much as other factors, such as SNR and the number of snapshots. So the DL-based methods have stable

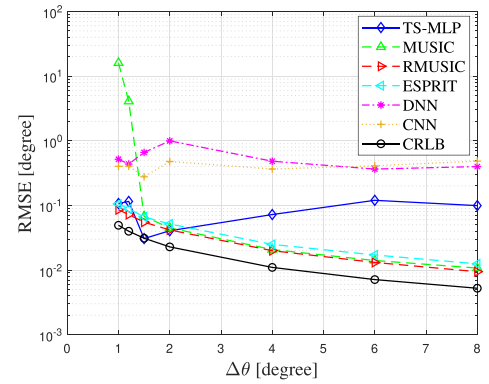


Fig. 13. RMSE versus angular interval  $\Delta\theta$  in DOA estimation of two sources at 15 dB SNR using  $L = 1,000$  snapshots.

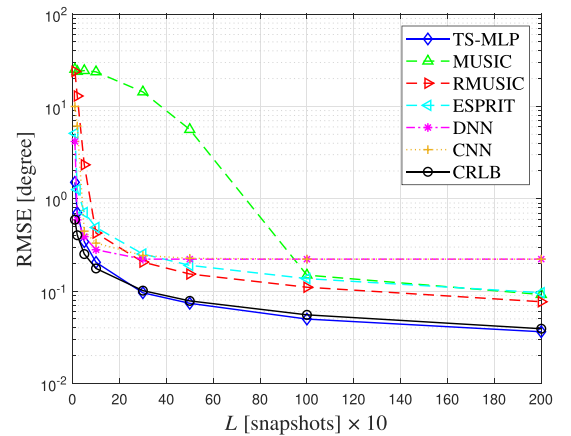


Fig. 14. RMSE versus number of snapshots  $L$  in DOA estimation of two sources at 5 dB SNR.

performance at different angle intervals. The fluctuation in the figure is probably caused by the number of training samples at different angle intervals.

3) *RMSE Versus Number of Snapshots  $L$* : Finally, the DOA estimation performance of each method is evaluated under different number of snapshots. The SNR is set to 5 dB while the numbers of snapshots tested are  $L = \{10, 20, 50, 100, 300, 500, 1,000, 2,000\}$ , the RMSE curves are plotted in Fig. 14. It can be seen that DNN and CNN methods perform the worst for a large number of snapshots, because they reach the upper limit soon. Also, the CNN produces high RMSE in the case of small snapshots, because it uses the entire covariance matrix as the input which is severely affected by the reduction of snapshots. Compared with other traditional methods, TS-MLP method has obvious advantages in all tested snapshot situations. It not only has better adaptability for a small number of snapshots, but also achieve smaller RMSE when using multiple snapshots and even approach or defeat CRLB. The possible reason is that it is a data-driven end-to-end DL-based estimator and is not unbiased. In general, the TS-MLP method can well meet the DOA estimation requirements in the case of small snapshots, and it can be further improved when the number of snapshots is sufficient.

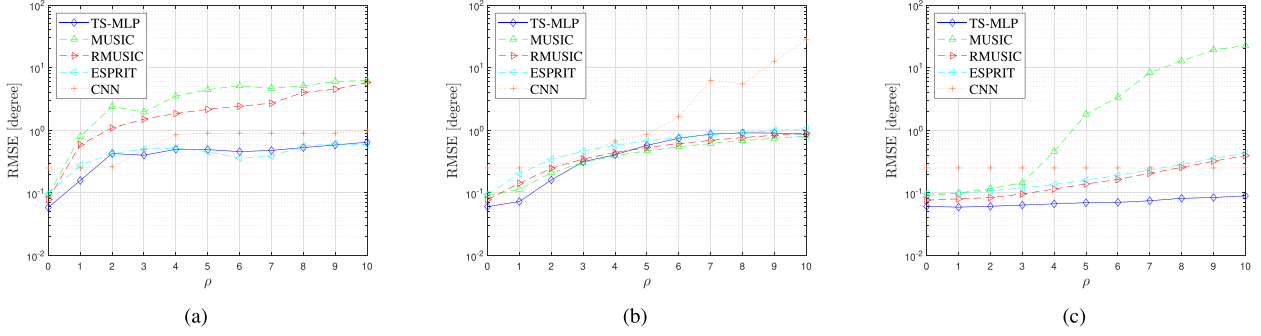


Fig. 15. DOA estimation RMSE for two signals from the directions of  $-1.25^\circ$  and  $1.25^\circ$  in the presence of different array imperfections at 10 dB using  $L = 500$  snapshots. There is no array imperfection in the training stage, but test dataset has array imperfections. (a) gain and phase errors, (b) mutual coupling error and (c) array element position error.

#### D. Robustness to Array Imperfections

In this subsection, we assess the generalization capability of the proposed method to array imperfections described in Section IV-B. It should be noted that the proposed method does not consider array imperfection in the training stage. All three imperfections only appear during testing. We assume that two signals from the directions  $\theta_1 = -1.25^\circ$  and  $\theta_2 = 1.25^\circ$  impinge onto the array with SNR = 10 dB. Herein, the covariance matrix is calculated by  $L = 500$  snapshots for all three cases.

Just like the experiment in [24], we adjust the parameter  $\rho$  in (11)–(14) from 0 to 1 to change the array imperfection conditions. Three cases with different array imperfections are considered by setting  $\delta_{(\cdot)}$  in (15) to different values. First, we set  $\delta_g = \delta_p = 1$  and  $\delta_{mc} = \delta_{ps} = 0$ , i.e., only gain and phase errors are considered. When  $\rho$  varies from 0 to 1, the RMSEs of the DOA estimates in 1,000 independent simulations are shown in Fig. 15(a). Then, we set  $\delta_g = \delta_p = \delta_{ps} = 0$  and  $\delta_{mc} = 1$ , thus only mutual coupling error exists, and the corresponding RMSEs are shown in Fig. 15(b). Finally, we set  $\delta_g = \delta_p = \delta_{mc} = 0$  and  $\delta_{ps} = 1$  to retain the array element position error only, and the DOA estimation RMSEs are shown in Fig. 15(c).

As can be observed in Fig. 15(a), when the gain and phase errors appear, the performance of TS-MLP is better than CNN in most cases, close to ESPRIT method and significantly better than the other two traditional methods, MUSIC and RMUSIC. Specifically, when the gain and phase errors increase, and the proposed method is more stable than the other methods.

In Fig. 15(b), when the mutual coupling error exists, TS-MLP is the least affected when the error is small, but the impact will be slightly stronger than the other three traditional methods when the error increases. Generally, its performance is still better and more robust than that of the CNN method. As the mutual coupling error becomes larger, such as  $\rho \geq 9$ , the RMSE of TS-MLP gradually becomes comparable with the three conventional methods. On the contrary, when the error becomes large, the RMSE of CNN deviates greatly.

Finally, if there is element position error, as shown in Fig. 15(c), TS-MLP is always superior to CNN and three conventional methods. With the increase of errors, the robustness of TS-MLP is obviously better than the MUSIC method,

and more stable than other traditional methods. Although the proposed method is not trained for any kinds of array imperfection, it still shows robust performance, which is comparable with the conventional methods and better than the CNN method, and no excessive RMSE appears due to array imperfections.

#### VI. CONCLUSION

In this paper, we proposed the TS-MLP network to deal with the DOA estimation problem with a finer grid resolution than previous DL based methods. Our MLP framework consists of three parts with one input and three outputs. The super-resolution DOA estimation procedure was divided into three steps: first, the integer-degree angle region was determined where the signal source angle is located; second, more accurate information of the decimal-degree angle was obtained; third, the two estimates of multiple sources were paired to obtain the final estimation results. In this way, a higher resolution grid, i.e.,  $0.01^\circ$ , was realized without greatly increasing the output length and the number of parameters for training. The training data used, which match practical cases and were closer to the general signals, retain the decimal-degree DOAs of two sources. Compared with several traditional methods, such as MUSIC, RMUSIC, and ESPRIT, the proposed solution had generalization ability, simple operation, and is more computationally efficient. Compared with other DL methods, the proposed solution achieved higher resolution. In addition, the proposed method adapted to low SNRs, closely separated angles and limited number of snapshots.

However, the proposed method also faces a serious problem. Due to the finer grid and the consideration of more general DOA angle pairs, it means that the number of DOAs to be considered would be greatly increased, especially if it is to be extended to multiple sources. So possible future research directions can be focused on how to use less training samples to obtain a robust high-resolution DOA estimation network.

#### ACKNOWLEDGMENT

The authors would like to thank the anonymous reviewers for their insightful comments and suggestions.

## REFERENCES

- [1] H. Krim and M. Viberg, "Two decades of array signal processing research: The parametric approach," *IEEE Signal Process. Mag.*, vol. 13, no. 4, pp. 67–94, Jul. 1996.
- [2] S. Ge, K. Li, and S. N. B. M. Rum, "Deep learning approach in DOA estimation: A systematic literature review," *Mobile Inf. Syst.*, vol. 2001, 2001, Art. no. 6392875.
- [3] R. Schmidt, "A signal subspace approach to multiple emitter location spectral estimation," Ph.D. dissertation, Stanford Univ., Stanford, CA, USA, 1981.
- [4] A. Barabell, "Improving the resolution performance of eigenstructure-based direction-finding algorithms," in *Proc. IEEE Int. Conf. Acoust., Speech, Signal Process.*, 1983, pp. 336–339.
- [5] R. Roy, A. Paulraj, and T. Kailath, "Estimation of signal parameters via rotational invariance techniques - ESPRIT," in *Proc. IEEE Mil. Commun. Conf.: Commun.-Comput.: Teamed 90's*, 1986, pp. 41.6.1–41.6.5.
- [6] R. Roy and T. Kailath, "ESPRIT-estimation of signal parameters via rotational invariance techniques," *IEEE Trans. Acoust., Speech, Signal Process.*, vol. 37, no. 7, pp. 984–995, Jul. 1989.
- [7] P. Stoica and A. Nehorai, "MUSIC, maximum likelihood, and Cramer-Rao bound," *IEEE Trans. Acoust., Speech, Signal Process.*, vol. 37, no. 5, pp. 720–741, May 1989.
- [8] R. Kumaresan and D. W. Tufts, "Estimating the angles of arrival of multiple plane waves," *IEEE Trans. Aerosp. Electron. Syst.*, vol. AES-19, no. 1, pp. 134–139, Jan. 1983.
- [9] M. Viberg, B. Ottentent, and T. Kailath, "Direction-of-arrival estimation and detection using weighted subspace fitting," in *Proc. 23rd Asilomar Conf. Signals, Syst. Comput.*, 1989, pp. 604–608.
- [10] X. Wu, W. P. Zhu, and J. Yan, "A Toeplitz covariance matrix reconstruction approach for direction-of-arrival estimation," *IEEE Trans. Veh. Technol.*, vol. 66, no. 9, pp. 8223–8237, Sep. 2017.
- [11] W. Zhang, P. Wang, N. He, and Z. He, "Super resolution DOA based on relative motion for FMCW automotive radar," *IEEE Trans. Veh. Technol.*, vol. 69, no. 8, pp. 8698–8709, Aug. 2020.
- [12] R. Akter, V.-S. Doan, T. Huynh-The, and D.-S. Kim, "RFDOA-Net: An efficient convnet for RF-based DOA estimation in UAV surveillance systems," *IEEE Trans. Veh. Technol.*, vol. 70, no. 11, pp. 12209–12214, Nov. 2021.
- [13] C. Liu and H. Zhao, "Efficient DOA estimation method using bias-compensated adaptive filtering," *IEEE Trans. Veh. Technol.*, vol. 69, no. 11, pp. 13087–13097, Nov. 2020.
- [14] W. S. McCulloch and W. Pitts, "A logical calculus of the ideas immanent in nervous activity," *Bull. Math. Biol.*, vol. 52, pp. 99–115, 1990.
- [15] Y. LeCun, Y. Bengio, and G. Hinton, "Deep learning," *Nature*, vol. 521, no. 7553, pp. 436–444, 2015.
- [16] F. Rosenblatt, "The perceptron: A probabilistic model for information storage and organization in the brain," *Psychol. Rev.*, vol. 65, no. 6, pp. 386–408, 1958.
- [17] D. E. Rumelhart, G. E. Hinton, and R. J. Williams, "Learning representations by back-propagating errors," *Nature*, vol. 323, no. 6088, pp. 533–536, 1986.
- [18] H. Huang, J. Yang, H. Huang, Y. Song, and G. Gui, "Deep learning for super-resolution channel estimation and DOA estimation based massive MIMO system," *IEEE Trans. Veh. Technol.*, vol. 67, no. 9, pp. 8549–8560, Sep. 2018.
- [19] Y. Zheng, Y. Xiao, Z. Ma, P. D. Diamantoulakis, and G. K. Karagiannis, "Neural network-based multi-DOA tracking for high speed railway communication systems," *IEEE Trans. Veh. Technol.*, vol. 71, no. 10, pp. 11284–11288, Oct. 2022.
- [20] Z. Guo, K. Lin, X. Chen, and C.-Y. Chit, "Transfer learning for angle of arrivals estimation in massive MIMO system," in *Proc. IEEE/CIC Int. Conf. Commun. China*, 2022, pp. 506–511.
- [21] G. K. Papageorgiou, M. Sellathurai, and Y. C. Eldar, "Deep networks for direction-of-arrival estimation in low SNR," *IEEE Trans. Signal Process.*, vol. 69, pp. 3714–3729, 2021.
- [22] Y. Kase, T. Nishimura, T. Ohgane, Y. Ogawa, D. Kitayama, and Y. Kishiyama, "DOA estimation of two targets with deep learning," in *Proc. 15th Workshop Positioning, Navigation, Commun.*, 2018, pp. 1–5.
- [23] J. Yu, W. W. Howard, D. Tait, and R. M. Buehrer, "Direction-of-arrival estimation with a vector sensor using deep neural networks," in *Proc. IEEE 93rd Veh. Technol. Conf.*, 2021, pp. 1–7.
- [24] Z. Liu, C. Zhang, and P. S. Yu, "Direction-of-arrival estimation based on deep neural networks with robustness to array imperfections," *IEEE Trans. Antennas Propag.*, vol. 66, no. 12, pp. 7315–7327, Dec. 2018.
- [25] A. M. Ahmed, O. Eissa, and A. Sezgin, "Deep autoencoders for DOA estimation of coherent sources using imperfect antenna array," in *Proc. 3rd Int. Workshop Mobile Terahertz Syst.*, 2020, pp. 1–5.
- [26] L. Wu, Z. Liu, and Z. Huang, "Deep convolution network for direction of arrival estimation with sparse prior," *IEEE Signal Process. Lett.*, vol. 26, no. 11, pp. 1688–1692, Nov. 2019.
- [27] W. Zhu and M. Zhang, "A deep Learning architecture for broadband DOA estimation," in *Proc. IEEE 19th Int. Conf. Commun. Technol.*, 2019, pp. 244–247.
- [28] A. M. Ahmed, U. S. K. P. M. Thanthrige, A. E. Gamal, and A. Sezgin, "Deep learning for DOA estimation in MIMO radar systems via emulation of large antenna arrays," *IEEE Commun. Lett.*, vol. 25, no. 5, pp. 1559–1563, May 2021.
- [29] J. Cong, X. Wang, M. Huang, and L. Wan, "Robust DOA estimation method for MIMO radar via deep neural networks," *IEEE Sensors J.*, vol. 21, no. 6, pp. 7498–7507, Mar. 2021.
- [30] S. Chakrabarty and E. A. P. Habets, "Broadband DOA estimation using convolutional neural networks trained with noise signals," in *Proc. IEEE Workshop Appl. Signal Process. to Audio Acoust.*, 2017, pp. 136–140.
- [31] S. Adavanne, A. Politis, and T. Virtanen, "Direction of arrival estimation for multiple sound sources using convolutional recurrent neural network," in *Proc. IEEE 26th Eur. Signal Process. Conf.*, 2018, pp. 1462–1466.
- [32] R. Takeda and K. Komatani, "Discriminative multiple sound source localization based on deep neural networks using independent location model," in *Proc. IEEE Spoken Lang. Technol. Workshop*, 2016, pp. 603–609.
- [33] J. S. Jeong, K. Araki, and J.-I. Takada, "A neural network for direction of arrival estimation under coherent multiple waves," in *Proc. IEEE Asia-Pacific Conf. Circuits Syst. Microelectron. Integrating Syst.*, 1998, pp. 495–498.
- [34] H. Xiang, B. Chen, M. Yang, and S. Xu, "Angle separation learning for coherent DOA estimation with deep sparse prior," *IEEE Commun. Lett.*, vol. 25, no. 2, pp. 465–469, Feb. 2021.
- [35] R. Girshick, J. Donahue, T. Darrell, and J. Malik, "Rich feature hierarchies for accurate object detection and semantic segmentation," in *Proc. IEEE Conf. Comput. Vis. Pattern Recognit.*, 2014, pp. 580–587.
- [36] J. Redmon, S. Divvala, R. Girshick, and A. Farhadi, "You only look once: Unified, real-time object detection," in *Proc. IEEE Conf. Comput. Vis. Pattern Recognit.*, 2016, pp. 779–788.
- [37] T. Bai, "Analysis on two-stage object detection based on convolutional neural networks," in *Proc. IEEE Int. Conf. Big Data, Artif. Intell. Softw. Eng.*, 2020, pp. 321–325.
- [38] H. Xiang, B. Chen, T. Yang, and D. Liu, "Improved de-multipath neural network models with self-paced feature-to-feature learning for DOA estimation in multipath environment," *IEEE Trans. Veh. Technol.*, vol. 69, no. 5, pp. 5068–5078, May 2020.
- [39] K. Hornik, M. Stinchcombe, and H. White, "Multilayer feedforward networks are universal approximators," *Neural Netw.*, vol. 2, no. 5, pp. 359–366, 1989.
- [40] D. E. Rumelhart, R. Durbin, R. Golden, and Y. Chauvin, "Backpropagation: The basic theory," in *Backpropagation: Theory, Architecture, and Applications*, Y. Chauvin and D. E. Rumelhart, Eds., Hillsdale, NJ, USA, 1995, pp. 1–34.
- [41] D. P. Kingma and J. Ba, "Adam: A method for stochastic optimization," in *Proc. Int. Conf. Learn. Representations*, San Diego, CA, May 2015.
- [42] M. Zhang and Z. D. Zhu, "DOA estimation with sensor gain, phase and position perturbations," in *Proc. IEEE Nat. Aerosp. Electron. Conf.*, 1993, pp. 67–69.
- [43] Y. Li and M. H. Er, "Theoretical analyses of gain and phase error calibration with optimal implementation for linear equispaced array," *IEEE Trans. Signal Process.*, vol. 54, no. 2, pp. 712–723, Feb. 2006.
- [44] A. Paulraj and T. Kailath, "Direction of arrival estimation by eigenstructure methods with unknown sensor gain and phase," in *Proc. IEEE Int. Conf. Acoust., Speech, Signal Process.*, 1985, pp. 640–643.
- [45] B. Friedlander and A. J. Weiss, "Direction finding in the presence of mutual coupling," *IEEE Trans. Antennas Propag.*, vol. 39, no. 3, pp. 273–284, Mar. 1991.
- [46] A. J. Weiss and B. Friedlander, "Mutual coupling effects on phase-only direction finding," *IEEE Trans. Antennas Propag.*, vol. 40, no. 5, pp. 535–541, May 1992.
- [47] B. P. Flanagan and K. L. Bell, "Array self calibration with large sensor position errors," in *Proc. Conf. Rec. 33rd Asilomar Conf. Signals, Syst., Comput.*, 1999 pp. 258–262.





**Yanjun Zhang** received the B.S. degree in electronic information science and technology from Shandong University, Jinan, China. He is currently working toward the Ph.D. degree in electronic and information engineering with the State Key Laboratory of Millimeter Waves, Southeast University, Dhaka, Bangladesh. His research interests include signal processing, millimeter wave radar, target detection, and machine learning.



**Shiyang Tang** (Member, IEEE) was born in Jiangsu Province, China. He received the B.S. and Ph.D. degrees in electrical engineering from Xidian University, Xi'an, China, in 2011 and 2016, respectively. He is currently a Full Professor with the National Key Laboratory of Radar Signal Processing, Xidian University. His research interests include imaging of SAR with curved paths and high-speed moving target detection and imaging.



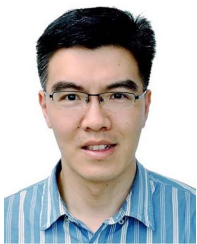
**Yan Huang** (Member, IEEE) received the B.S. degree in electrical engineering, and the Ph.D. degree in signal and information processing from Xidian University, Xi'an, China, in 2013 and 2018, respectively. He was a visiting Ph.D. student with the Electrical and Computer Engineering Department, University of Florida, Gainesville, FL, USA, from 2016 to 2017, and Electrical and Systems Engineering Department, Washington University in St. Louis, St. Louis, MO, USA, from 2017 to 2018. He is currently an Associate Professor with the State Key Laboratory of Millimeter

Waves, Southeast University, Dhaka, Bangladesh. His research interests include machine learning, synthetic aperture radar, image processing, and remote sensing.



**Hing Cheung So** (Fellow, IEEE) was born in Hong Kong. He received the B.Eng. degree in electronic engineering from the City University of Hong Kong, Hong Kong, in 1990, and the Ph.D. degree in electronic engineering from The Chinese University of Hong Kong, Hong Kong, in 1995. From 1990 to 1991, he was an Electronic Engineer with the Research and Development Division, Everex Systems Engineering Ltd., Hong Kong. From 1995 to 1996, he was a Postdoctoral Fellow with The Chinese University of Hong Kong. From 1996 to 1999, he was a Research

Assistant Professor with the Department of Electronic Engineering, City University of Hong Kong, where he is currently a Professor. His research interests include detection and estimation, fast and adaptive algorithms, multidimensional harmonic retrieval, robust signal processing, source localization, and sparse approximation. He was an elected Member of the Signal Processing Theory and Methods Technical Committee, IEEE Signal Processing Society, from 2011 to 2016, where he was the Chair of the Awards Subcommittee from 2015 to 2016. He has been on the editorial boards of *IEEE Signal Processing Magazine* from 2014 to 2017, *IEEE TRANSACTIONS ON SIGNAL PROCESSING* from 2010 to 2014, *Signal Processing* since 2010, and *Digital Signal Processing* since 2011. He was the Lead Guest Editor for the Special Issue on Advances in Time/Frequency Modulated Array Signal Processing of *IEEE JOURNAL OF SELECTED TOPICS IN SIGNAL PROCESSING* in 2017.



**Jun Tao** (Senior Member, IEEE) received the B.S. and M.S. degrees in electrical engineering from the Department of Radio Engineering, Southeast University, Nanjing, China, in 2001 and 2004, respectively, and the Ph.D. degree in electrical engineering from the Department of Electrical and Computer Engineering, University of Missouri, Columbia, MO, USA, in 2010. From 2004 to 2006, he was a System Design Engineer with Realsil Microelectronics Inc. (a subsidiary of Realtek), Suzhou, China. From 2011 to 2015, he was a Senior System Engineer with Qual-

comm Inc., Boulder, CO, USA, working on the baseband algorithm and architecture design for the UMTS/LTE modem. Since April 2016, he has been a Full Professor with the School of Information Science and Engineering, Southeast University, Nanjing, China. His research interests include the general areas of wireless cellular communications, underwater acoustic communications, and localization and tracking, including channel modeling and estimation, turbo equalization, adaptive filtering, Bayesian inference, and machine learning.



**Wei Hong** (Fellow, IEEE) received the B.S. degree in radio engineering from the University of Information Engineering, Zhengzhou, China, in 1982, and the M.S. and Ph.D. degrees in radio engineering from Southeast University, Nanjing, China, in 1985 and 1988, respectively. Since 1988, he has been with the State Key Laboratory of Millimeter Waves and serves for the Director of the lab since 2003. He is currently a Professor with the School of Information Science and Engineering, Southeast University. In 1993, 1995, 1996, 1997, and 1998, he was a short-term Visiting

Scholar with the University of California at Berkeley, Berkeley, CA, USA, and at Santa Cruz. He has authored and coauthored more than 300 technical publications and two books. His research interests include numerical methods for electromagnetic problems, millimeter wave theory and technology, antennas, and RF technology for wireless communications. He was twice the recipient of the awarded the National Natural Prizes, thrice awarded the first-class Science and Technology Progress Prizes issued by the Ministry of Education of China and Jiangsu Province Government, and Foundations for China Distinguished Young Investigators and for "Innovation Group" issued by NSF of China. He is a Fellow of CIE, the Vice Presidents of CIE Microwave Society and Antenna Society, the Chair of IEEE MTT-S/AP-S/EMC-S Joint Nanjing Chapter, and was an elected IEEE MTT-S AdCom Member during 2014–2016. From 2007 to 2010, he was an Associate Editor for *IEEE TRANSACTIONS ON MICROWAVE THEORY AND TECHNIQUES*.